PHYSICAL REVIEW D **92,** 094033 (2015)

Diphoton production at the Tevatron and the LHC in the NLO approximation of the parton Reggeization approach

M. A. Nefedov[*]
Samara State University, Ac. Pavlov st., 1, 443011 Samara, Russia

V. A. Saleev[†]
Samara State University, Academician Pavlov Street, 1, 443011 Samara, Russia
and S. P. Korolyov Samara State Aerospace University, Moscow Highway, 34, 443086 Samara, Russia
(Received 6 August 2015; published 25 November 2015)

The hadroproduction of prompt isolated photon pairs at high energies is studied in the framework of the parton Reggeization approach. The real part of the NLO corrections is computed (the NLO* approximation), and the procedure for the subtraction of double counting between real parton emissions in the hard-scattering matrix element and unintegrated parton distribution function is constructed for the amplitudes with Reggeized quarks in the initial state. The matrix element of the important next-to-next-to-leading-order subprocess $RR \to \gamma\gamma$ with full dependence on the transverse momenta of the initial-state Reggeized gluons is obtained. We compare obtained numerical results with diphoton spectra measured at the Tevatron and the LHC and find a good agreement of our predictions with experimental data at the high values of diphoton transverse momentum, p_T, and especially at the p_T larger than the diphoton invariant mass, M. In this multi-Regge kinematics region, the NLO correction is strongly suppressed, demonstrating the self-consistency of the parton Reggeization approach.

DOI: 10.1103/PhysRevD.92.094033 PACS numbers: 12.38.Bx, 12.39.St, 12.40.Nn, 13.87.Ce

I. INTRODUCTION

Nowadays, the inclusive hadroproduction of pairs of isolated prompt photons (diphotons) is a subject of intense experimental and theoretical studies. From the experimental point of view, this process forms an irreducible background in the searches of heavy neutral resonances in the diphoton decay channel, such as the Standard Model Higgs boson [1] and its beyond the Standard Model counterparts [2]. As for the process itself, it allows us to define the set of inclusive differential cross sections over such variables as the invariant mass of the pair (M), its transverse momentum (p_T), the azimuthal angle between transverse momenta of the photons ($\Delta\phi$), the rapidity of the photon pair ($Y_{\gamma\gamma}$), the Collins–Soper angle in the center-of-mass frame of the photon pair (θ), and a few others [3]. Most of these spectra are measured with high precision both at the Tevatron [3] and the LHC [4].

On the theoretical side, providing the predictions for the above-mentioned rich set of differential spectra is a challenging task even for the state-of-the-art techniques in perturbative QCD (pQCD), while for the inclusive isolated prompt photon production, the p_T-spectra from CDF [5], ATLAS [6], and CMS [7] are described within experimental uncertainties in the next-to-leading order (NLO) of the conventional collinear parton model (CPM) of QCD [8]. Also, the notably good results were obtained for these spectra already in the leading order (LO) of k_T factorization in Refs. [9,10]. In contrast, existing NLO CPM calculations, implemented in the DIPHOX [11] Monte Carlo event generator, provide a very poor description of p_T and $\Delta\phi$ distributions measured by ATLAS [4]. In the CPM, the full next-to-next-to-leading-order (NNLO) accuracy is required to provide a qualitatively reasonable description of all distributions [12].

Part of these difficulties can be traced back to the shortcomings of the CPM approximation, where the transverse momentum of initial-state partons is integrated over in the parton distribution functions (PDFs) but neglected in the hard-scattering part of the process. Such treatment is justified for the fully inclusive single-scale observables, such as deep inelastic scattering structure functions or p_T spectra of single prompt photons and jets, where the corrections breaking the collinear factorization are shown to be suppressed by powers of the hard scale [13].

For the multiscale differential observables, there is no obvious reason why the fixed-order calculation in the CPM should be a good approximation. Usually, the simple picture of factorization of the cross section of the hard process into the convolution of the hard-scattering coefficient and some PDF-like objects is kept, but kinematical approximations are relaxed. In the treatment of initial-state radiation (ISR) corrections in the soft collinear effective theory (SCET) [14] or in the transverse momentum-dependent (TMD) factorization formalism [13,15,16], the transverse momentum of the initial-state parton is kept unintegrated on the kinematical level but neglected in the

[*]nefedovma@gmail.com
[†]saleev@samsu.ru

hard-scattering part, which is justified e.g., when the p_T of the exclusive final state is much smaller than its invariant mass, so that the following hierarchy of the light-cone momentum components for the initial-state parton is preserved: $q^{\mp} \ll |\mathbf{q}_T| \ll q^{\pm} = x\sqrt{S}$.

In the opposite limit, when $q^{\mp} \ll |\mathbf{q}_T| \sim q^{\pm} = x\sqrt{S}$, the k_T factorization [17] is valid, and the transverse momentum of the initial-state parton can no longer be neglected in the hard-scattering amplitudes. To obtain the suitable hard-scattering matrix element, we will apply the hypothesis of parton Reggeization, which will be described below. In what follows, we will refer to the combination of k_T factorization with hard-scattering matrix elements with Reggeized partons in the initial state as the parton Reggeization approach (PRA). This approach is mostly suitable for the study of the production of the final states with high p_T and small invariant mass in the central rapidity region. At high energies $\sqrt{S} \gg p_T$, such final states are produced by the small-x partons, and the resummation of $\log(1/x)$-enhanced terms into the unintegrated PDF (unPDF) can be implemented [18]. Clearly, the regions of applicability of the TMD and k_T factorization are overlapping, and they should match when $x \to 1$, so we propose the hybrid factorization scheme which uses the k_T-factorization formula and interpolates smoothly between the TMD and k_T-factorization momentum regions. The effects of ISR with small k_T or highly separated in rapidity from the central region are included into unPDFs in PRA, while the radiation close in rapidity to the central region should be included order by order in α_s.

Turning back to the photon pair production, we can conclude that neither TMD nor k_T factorization covers all the available range of experimental data, so our hybrid approach will be especially suitable for this observable. Most of the cross section comes from the region where the diphoton has small p_T and photons fly nearly back to back in the transverse plane, so additional QCD radiation is kinematically constrained to be soft and collinear, and the approach of SCET factorization will be preferable. On the contrary, at high p_T and small $\Delta\phi$, already the LO in PRA will do a good job, as we will show below.

The previous attempts to study the prompt diphoton production in k_T factorization [19,20] had their own problems. In Ref. [19], only LO $2 \to 2$ subprocesses were taken into account. While, the PRA was used to obtain the gauge-invariant expression for the $Q\bar{Q} \to \gamma\gamma$ matrix element with off-shell initial-state Reggeized quarks (Q), the matrix element for the $RR \to \gamma\gamma$ with off-shell Reggeized gluons in the initial state was taken the same as in the CPM. In fact, this contribution was overestimated in Ref. [19] due to the erroneous overall factor 4 in the partonic cross section of the subprocess $gg \to \gamma\gamma$ presented in Ref. [21], which lead to the accidental agreement with the early Tevatron data [22]. This factor was carefully checked against the results presented in the literature [23,24], as well as by our independent calculations of the exact $RR \to \gamma\gamma$ amplitude, described in Sec. IV of the present paper.

In Ref. [20], the attempt to take into account the NLO $2 \to 3$ subprocesses was made, but manifestly nongauge-invariant matrix elements were used both for $2 \to 2$ and $2 \to 3$ subprocesses. Also, the unavoidable double counting of additional real radiations between NLO $q^\star g^\star \to q\gamma\gamma$ subprocess and the unPDF was not subtracted, which has lead to the questionable conclusion that no resummation of the effects of soft radiation is needed in the small-p_T region to describe the data.

In view of the above-mentioned shortcomings of the previous calculations, the present study has two main goals. The first one is to calculate the real part of NLO corrections to the process under consideration in the PRA, and develop the technique of subtraction of double counting between real NLO corrections and unPDF in PRA. By the NLO* approximation in PRA, we mean the combination of the real part of NLO corrections with the proper double-counting subtraction technique. The second goal is to calculate the matrix element of the quark-box subprocess $RR \to \gamma\gamma$ in PRA, taking into account the exact dependence on the transverse momenta of initial-state Reggeized gluons.

The present paper has the following structure. In Sec. II, the relevant basics of the PRA formalism are outlined, and the amplitude for the LO subprocess $Q\bar{Q} \to \gamma\gamma$ is derived. In Sec. III, the NLO $2 \to 3$ amplitudes are derived, and the procedure for the subtraction of double counting between NLO real corrections and unPDF is explained. In Sec. IV, the computation of the amplitude for the quark-box subprocess $RR \to \gamma\gamma$ is reviewed, and in Sec. V, we compare our numerical results with the most recent CDF [3] and ATLAS [4] data. Our conclusions are summarized in Sec. VI.

II. BASIC FORMALISM AND LO CONTRIBUTION

As collinear factorization is based on the property of factorization of collinear singularities in QCD [25], the k_T factorization is based on the Balitsky–Fadin–Kuraev–Lipatov (BFKL) [26] (see Refs. [27,28] for the review) factorization of QCD amplitudes in the multi-Regge kinematics (MRK), i.e., in the limit of the high scattering energy and fixed momentum transfers. For example, the amplitude for the subprocess $q(q_1) + q(q_2) \to q(q_3) + g(q_4) + q(q_5)$ in the limit when

$$s_{34} \gg -t_{13}, \qquad s_{45} \gg -t_{25},$$

where $s_{ij} = (q_i + q_j)^2$, $t_{ij} = (q_i - q_j)^2$, has the form of the amplitude with the exchange of the effective Reggeized particle in the t channel,

$$\mathcal{A}^{c,\mu} = 2s(\bar{u}(q_3)\gamma^{r_1}u(q_1)) \cdot \frac{1}{t_{13}}\left(\frac{s_{34}}{s_0}\right)^{\omega(t_{13})} \cdot \Gamma^{c,\mu}_{r_1 r_2}(q_{t1}, q_{t2}) \cdot \frac{1}{t_{25}}\left(\frac{s_{45}}{s_0}\right)^{\omega(t_{25})} \cdot (\bar{u}(q_5)\gamma^{r_2}u(q_2)), \tag{1}$$

where $q_{t1} = q_1 - q_3$, $q_{t2} = q_5 - q_2$, c, r_1, and r_2 are the color indices; γ^r is the effective qqR vertex; $\Gamma^{c,\mu}_{r_1,r_2}(q_{t1}, q_{t2})$ is the central gluon production vertex RRg; and $\omega(t)$ is the gluon Regge trajectory. The Slavnov–Taylor identity $(q_{t1} - q_{t2})_\mu \Gamma^{c,\mu}_{r_1 r_2}(q_{t1}, q_{t2}) = 0$ holds for the effective production vertex, which ensures the gauge invariance of the amplitude.

The analogous form for the MRK asymptotics of the amplitude with the quark exchange in the t channel was shown to hold in the leading logarithmic approximation (LLA) in Ref. [29]. For the review of the modern status of the quark Reggeization in QCD, see Ref. [30].

The Regge factor $s^{\omega(t)}$ resums the loop corrections enhanced by the $\log(s)$ to all orders in the strong coupling constant α_s, and the dependence on the arbitrary scale s_0 should be canceled by the analogous dependence of the effective vertices, taken in all orders of perturbation theory. The Reggeized gluon in the t channel is a scalar particle in the adjoint representation of the $SU(N_c)$. In the MRK limit, when all three particles in the final state are highly separated in rapidity, the light-cone momentum components carried by the Reggeons in t channels obey the hierarchy $q_t^\mp \ll |\mathbf{q}_{t\perp}| \sim q_t^\pm$, so in the strict MRK limit, the "small" light-cone component is usually neglected.

To go beyond the LLA in $\log(s)$, one needs to consider the processes with a few clusters of particles in the final state, which are highly separated in rapidity, but keeping the exact kinematics within clusters. This is the so-called quasi-multi-Regge kinematics(QMRK), and to obtain the amplitudes in this limit, the gauge-invariant effective action for high-energy processes in QCD was introduced in Ref. [31]. Apart from the usual quark and gluon fields of QCD, which are supposed to live within a fixed rapidity interval, the fields of Reggeized gluons [31] and Reggeized quarks [32] are introduced to communicate between the different rapidity intervals. To keep the t channel factorized form of the amplitudes in the QMRK limit, the Reggeon fields have to be gauge invariant, which leads to the specific form of their nonlocal interaction with the usual QCD fields, containing the Wilson lines. Gauge invariance of Reggeon fields also ensures the gauge invariance of the effective emission vertices, which describe the production of particles within the given interval of rapidity, as it was the case in (1). The Feynman rules (FRs) of the effective theory are collected in Refs. [32,33], but for the reader's convenience, we also list the FRs relevant for the purposes of the present study in Fig. 1. To compute the hard-scattering matrix elements in PRA, one has to combine the FRs of Fig. 1 with the usual FRs of QCD and QED and use the factors for the Reggeons in the initial state of the hard subprocess, also defined in Fig. 1 to be compatible with the normalization of the unPDF described below.

Recently, the new scheme to obtain gauge-invariant matrix elements for k_T factorization by exploiting the spinor-helicity representation and recursion relations for the tree-level amplitudes was introduced [34,35]. This technique is equivalent to the PRA for the tree-level amplitudes without internal Reggeon propagators; however, the construction of the subtraction terms in Sec. III requires the usage of the FRs of Refs. [32,33].

Since, the form of the central production vertex, propagators of Reggeized gluons and Regge trajectories, depends only on the quantum numbers of the Reggeon in the t channel and do not depend on what particles are in the initial state, the cross section of the production of particles to the central rapidity region in the inelastic pp collisions can be written in the form [17],

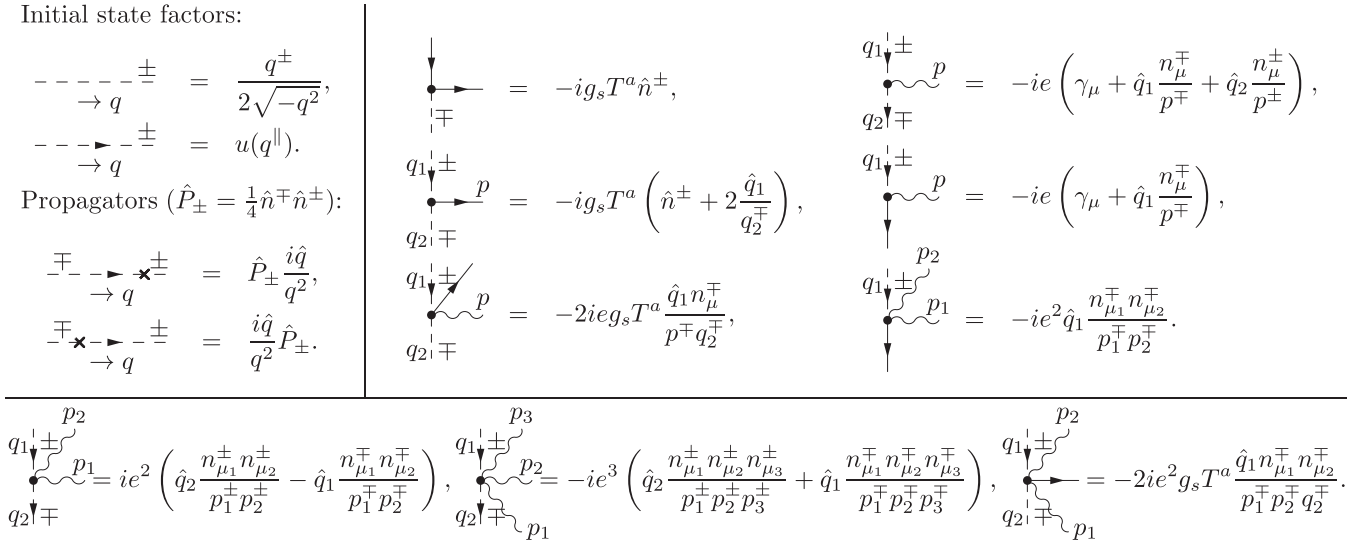

FIG. 1. The Feynman rules of the effective theory [31,32], relevant for the present study. The propagators; factors, corresponding to the Reggeized quarks (dashed lines with arrows); and gluons (dashed lines) in the initial state of the hard subprocess and necessary interaction vertices are presented. All momenta for the vertices are incoming.

$$d\sigma = \sum_{i,j} \int \frac{dx_1}{x_1} \int \frac{d^2\mathbf{q}_{T1}}{\pi} \Phi_i(x_1, t_1, \mu_F^2) \times \int \frac{dx_2}{x_2} \int \frac{d^2\mathbf{q}_{T2}}{\pi} \Phi_j(x_2, t_2, \mu_F^2) d\hat{\sigma}_{ij}(q_1, q_2), \quad (2)$$

where the sums are taken over the parton species, $q_{1,2} = x_{1,2}P_{1,2} + q_{T1,2}$ are the momenta of the partons, $q_{1,2}^2 = -\mathbf{q}_{T1,2}^2 = -t_{1,2}$, $P_{1,2}$ are the 4-momenta of the protons, $2P_1P_2 = S$, and $d\hat{\sigma}$ is the partonic cross section with Reggeized partons in the initial state. In what follows, we will often use the Sudakov decomposition of the momenta,

$$k = \frac{1}{2}(n^+k^- + n^-k^+) + k_T,$$

where $k^\pm = k^0 \pm k^3$, $P_1 = \sqrt{S}n^-/2$, $P_2 = \sqrt{S}n^+/2$, $(n^+)^2 = (n^-)^2 = 0$, $n^+n^- = 2$.

The unPDF $\Phi_i(x, \mathbf{q}_T^2, \mu_F^2)$ is unintegrated over the transverse momentum $\mathbf{q}_T^2$ but still integrated over the small light-cone component of momentum, so this light-cone component is neglected in the hard-scattering part, which is hence *formally* in the QMRK with the ISR and therefore is gauge invariant. The exact kinematics will be restored by the higher-order QMRK corrections. The factorization scale μ_F^2 is introduced to keep track of the position of the hard process on the axis of rapidity.

The unPDF is normalized on the CPM number density PDF via

$$\int^{\mu_F^2} dt \Phi_i(x, t, \mu_F^2) = x f_i(x, \mu_F^2).$$

In the case of an inelastic scattering of objects with an intrinsic hard scale, such as photons with a high center-of-mass energy and virtuality, the evolution of the unPDFs is governed by the large $\log(1/x)$, and they satisfy the BFKL evolution equation [26]. In proton-proton collisions, the initial state does not provide us with an intrinsic hard scale, and therefore the k_T-ordered Dokshitzer–Gribov–Lipatov–Altarelli–Parisi (DGLAP) [36] evolution at small k_T should be merged with rapidity-ordered BFKL evolution at high-k_T final steps of the ISR cascade.

The last problem is highly nontrivial and equivalent to the complete resummation of the $\log(k_T)$-enchanced terms in the BFKL kernel. A few phenomenological schemes to compute unPDFs of a proton were proposed, such as the Ciafaloni-Catani-Fiorani-Marchesini (CCFM) approach [18], the Blümlein approach [37], and the Kimber-Martin-Ryskin (KMR) approach [38]. In the LO calculations in PRA, the definition of the hard-scattering coefficient $d\hat{\sigma}$ is independent on the approximations made in the unPDF, so any unPDF can be used, and the spread between them gives the theoretical uncertainty. In fact, the recent studies [39,40] show that in the realistic kinematical conditions the LO calculations with KMR and a recent version of the CCFM unPDFs [41] give very close results. At the NLO, one should develop the proper matching scheme between the unPDF and corrections included into the hard-scattering kernel, which introduces a difference in the treatment of different unPDFs.

In the present paper, we will work with the version of the KMR formula for the unPDFs, described in Ref. [42]. The KMR prescription introduces the simplest possible scenario, where the k_T-ordered DGLAP chain of the emissions is followed by exactly one emission, ordered in rapidity with the particles produced in the hard subprocess. Because of the strong k_T ordering of the DGLAP evolution, the transverse momentum of the parton in the initial state of the hard subprocess is approximated to come completely from the last step of the evolution. With these approximations, one can obtain the unPDF from the conventional collinear PDF as

$$\Phi_i(x, q_T^2, \mu^2) = \frac{1}{q_T^2} \int_x^1 dz T_i(q^2, \mu^2) \frac{\alpha_s(q^2)}{2\pi} \times \sum_j P_{ij}(z) f_j\left(\frac{x}{z}, q^2\right) \theta(\Delta_{ij}(q_T^2, \mu^2) - z), \quad (3)$$

where $P_{ij}(z)$ is the DGLAP splitting function, $q^2 = q_T^2/(1-z)$ is the virtuality of the parton in the t channel, the Sudakov formfactor T_i is defined as

$$T_i(q^2, \mu^2) = \exp\left\{ -\int_{q^2}^{\mu^2} \frac{dk^2}{k^2} \frac{\alpha_s(k^2)}{2\pi} \sum_{i,j} \int_0^1 d\xi \xi P_{ij}(\xi) \times \theta(\Delta_{ij}(k^2(1-\xi), \mu^2) - \xi) \right\}, \quad (4)$$

and the ordering in rapidity between the last parton emission and the particles produced in the hard subprocess is implemented via the following infrared cutoff [43]:

$$\Delta_{ij}(q_T^2, \mu^2) = \frac{\mu}{\mu + q_T} \delta_{ij} + (1 - \delta_{ij}).$$

In the present study, we use the version of the KMR formula (3) with LO DGLAP splitting functions but NLO PDFs as a collinear input because, as it was shown in Ref. [42], the usage of the NLO PDFs and the exact scale q^2 are the most numerically important effects distinguishing the LO KMR distribution of Ref. [38] and the NLO prescription of Ref. [42]. Also, as it will be shown in Sec. III, the usage of the LO DGLAP splitting functions is compatible with the PRA, while at the NLO, the splitting functions should be recalculated using the effective theory of Refs. [31,32].

The effects of the Sudakov resummation are known to be dominant in the doubly asymptotic region, $q_T \ll \mu$ and $z \to \Delta$, which is most important in pp collisions; therefore, we use the Sudakov form factor in (4). The opposite limit, when $z \to 0$ and $q_T \ll \mu$, is captured by the Regge factor $s^{\omega(t)}$, but the proper procedure of matching of the double-logarithmic corrections, between Sudakov and Regge factors, is also beyond the scope of the present study.

Now, we move from the general discussion of PRA to the computation of the LO and NLO contributions to the prompt photon pair production. In the standard k_T factorization, the quark-induced processes are often neglected because they are power supressed in the LO BFKL formalism. It is expected that at some very small x the contribution of valence quarks will become negligible and all sea quarks will be generated on the last step of the evolution, so it is better to include this last step into the hard subprocess and erase quark PDFs completely. However, in realistic kinematical conditions, this power supression is compensated by the smallness of α_s, DGLAP evolution effects, and the non-negligible distribution of valence quarks, so the Reggeized quark induced processes often play an important phenomenological role. There is only one LO $[O(\alpha^2\alpha_s^0)]$ subprocess:

$$Q(q_1) + \bar{Q}(q_2) \to \gamma(q_3) + \gamma(q_4). \tag{5}$$

The set of Feynman diagrams for this subprocess is presented in Fig. 2. The amplitude of the process (5) obeys the Ward identity of QED, and the amplitude squared and averaged over the spin and color quantum numbers of the initial state, which was obtained for the first time in Ref. [19], has the form

$$\overline{|\mathcal{A}(Q\bar{Q} \to \gamma\gamma)|^2} = \frac{32}{3}\pi^2 e_q^4 \alpha^2 \frac{x_1 x_2}{a_3 a_4 b_3 b_4 S \hat{t}\,\hat{u}} \times (w_0 + w_1 S + w_2 S^2 + w_3 S^3), \tag{6}$$

where $a_3 = q_3^+/\sqrt{S}$, $a_4 = q_4^+/\sqrt{S}$, $b_3 = q_3^-/\sqrt{S}$, $b_4 = q_4^-/\sqrt{S}$, $\hat{s} = (q_1 + q_2)^2$, $\hat{t} = (q_1 - q_3)^2$, $\hat{u} = (q_1 - q_4)^2$, $x_1 = a_3 + a_4$, $x_2 = b_3 + b_4$, $\alpha = e^2/(4\pi)$, e_q is the electric charge of the quark in the units of the electron charge, and the coefficients w_i can be represented as follows:

$$\begin{aligned}
w_0 &= t_1 t_2 (t_1 + t_2) - \hat{t}\,\hat{u}(\hat{t} + \hat{u}),\\
-w_1 &= t_1 t_2 (a_3 - a_4)(b_3 - b_4) + t_2 x_1 (b_4 \hat{t} + b_3 \hat{u})\\
&\quad + t_1 x_2 (a_3 \hat{t} + a_4 \hat{u})\\
&\quad + \hat{t}\,\hat{u}(a_3 b_3 + 2a_4 b_3 + 2a_3 b_4 + a_4 b_4),\\
-w_2 &= b_3 b_4 x_1^2 t_2 + a_3 a_4 x_2^2 t_1 + a_3 b_4 \hat{t}(x_2 a_3 + a_4 b_4)\\
&\quad + a_4 b_3 \hat{u}(a_3 b_3 + a_4 x_2),\\
-w_3 &= a_3 a_4 b_3 b_4 \left(a_3 b_4 \left(\frac{\hat{t}}{\hat{u}}\right) + a_4 b_3 \left(\frac{\hat{u}}{\hat{t}}\right)\right).
\end{aligned}$$

Taking the collinear limit $t_{1,2} \to 0$ of (6), one can reproduce the standard CPM result for the amplitude $q\bar{q} \to \gamma\gamma$:

$$\overline{|\mathcal{A}(q\bar{q} \to \gamma\gamma)|^2} = \frac{32}{3}\pi^2 e_q^4 \alpha^2 \left(\frac{\hat{t}}{\hat{u}} + \frac{\hat{u}}{\hat{t}}\right).$$

In the next section, we will discuss the tree-level NLO corrections.

III. REAL NLO CORRECTIONS

The tree-level NLO $[O(\alpha^2\alpha_s^1)]$ subprocesses are

$$Q(q_1) + R(q_2) \to \gamma(q_3) + \gamma(q_4) + q(q_5), \tag{7}$$

$$Q(q_1) + \bar{Q}(q_2) \to \gamma(q_3) + \gamma(q_4) + g(q_5). \tag{8}$$

The sets of Feynman diagrams for them are presented in Figs. 3 and 4. The FRs of Fig. 1 were implemented as the `ReggeQuarks` [44] model file for the `FeynArts` [45], `Mathematica` based package, and the computation of the squared matrix elements was performed using the `FeynArts`, `FeynCalc` [46], and `FORM` programs. It was checked analytically that the amplitudes for the NLO subprocesses (7) and (8) obey the Ward (Slavnov–Taylor) identities with respect to all final-state photons (gluons) independently of the transverse momentum of the

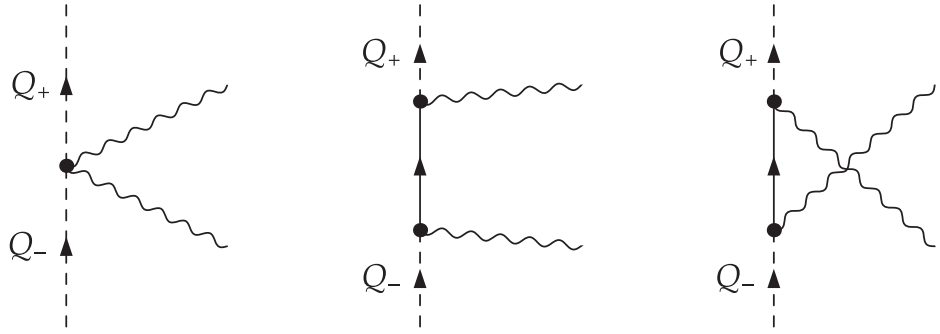

FIG. 2. The set of Feynman diagrams for the LO subprocess (5).

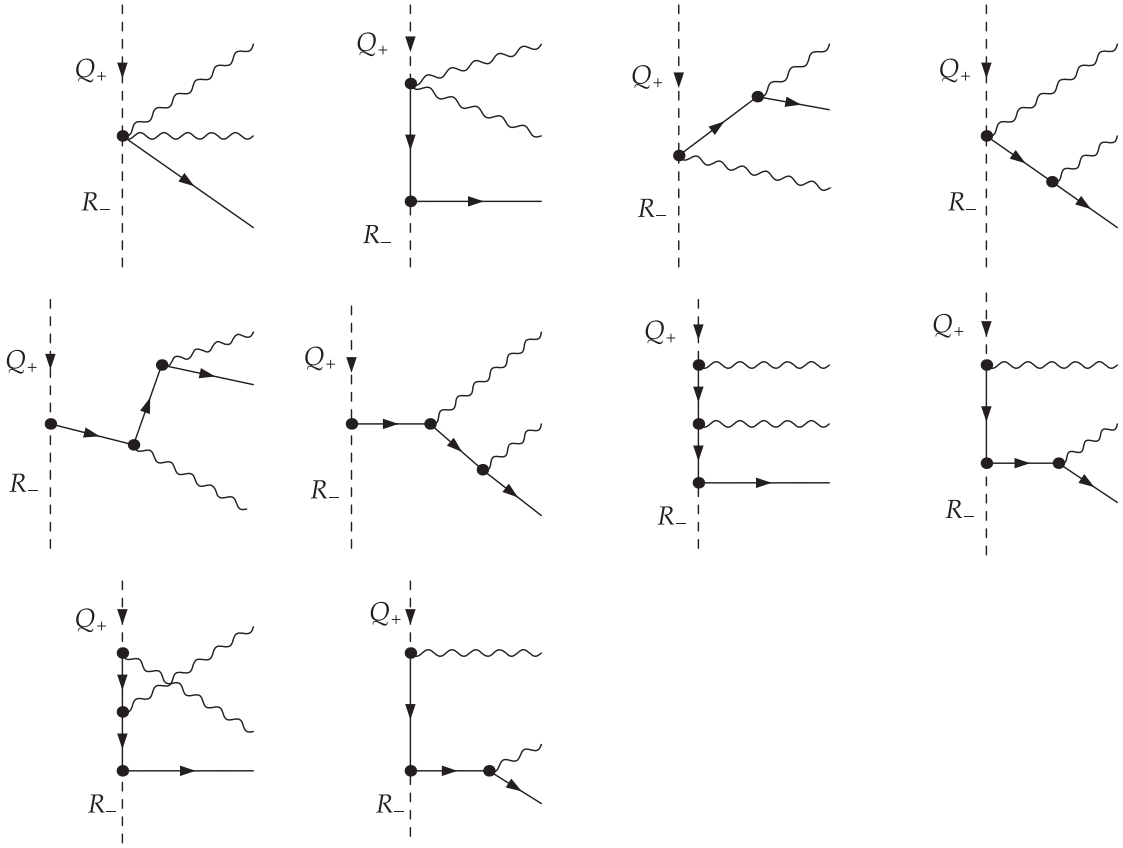

FIG. 3. The set of the Feynman diagrams for the NLO subprocess (7).

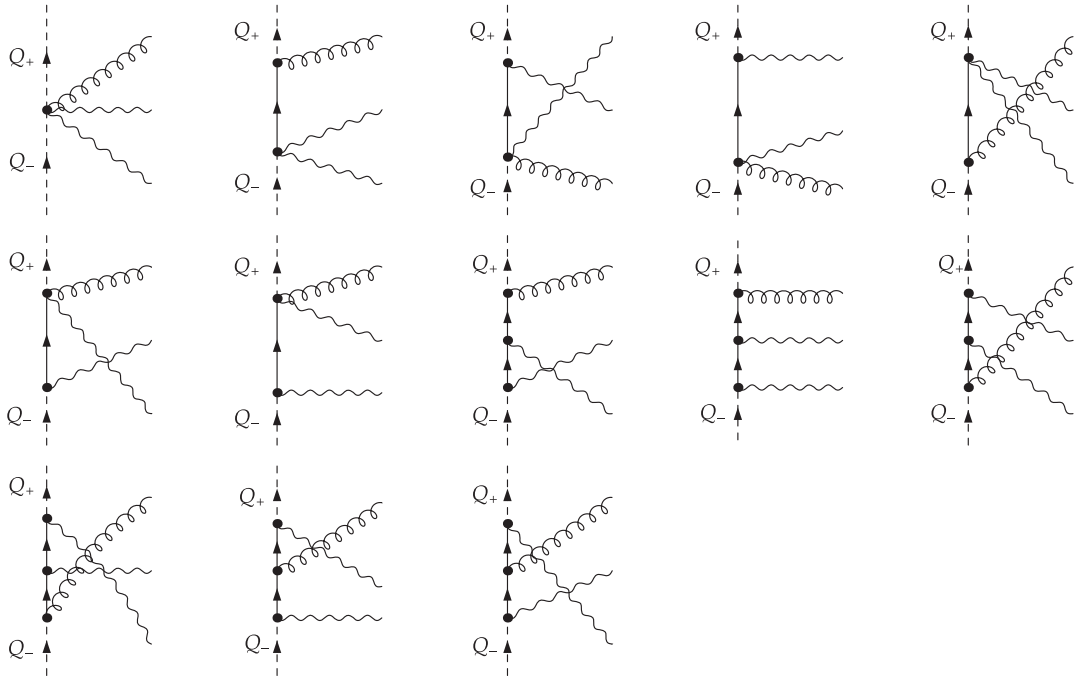

FIG. 4. The set of the Feynman diagrams for the NLO subprocess (8).

initial-state Reggeized partons. Unfortunately, the obtained expressions are too large and noninformative to present them here.

The squared matrix element of the subprocess (7) contains the collinear singularity, when the 3-momentum of the quark becomes collinear to the 3-momentum of one of the photons. This collinear singularity can be absorbed into the nonperturbative parton-to-photon fragmentation function, and then the theoretical cross section is represented as the sum of the *direct* contribution, where the collinear singularity is subtracted, according to e.g., the $\overline{\rm MS}$ scheme, and *fragmentation* contribution, which is equal to the convolution of the cross section of the parton production in pQCD and the parton-to-photon fragmentation function. The experimental (hard-cone) isolation condition requires the amount of hadronic energy within the photon isolation cone of the radius R to be smaller than the fixed value $E_T^{(\rm ISO)} \sim O(1)$ GeV,

$$E_T^{(\rm had)}(r < R) < E_T^{(\rm ISO)}, \tag{9}$$

where $r = \sqrt{\Delta\eta^2 + \Delta\phi^2}$ is the distance in the pseudorapidity–azimuthal angle plane and $E_T^{(\rm had)}(r < R)$ is the amount of the hadronic transverse energy within the isolation cone around the photon. This isolation condition strongly suppresses the fragmentation component, but at high energies, fragmentation is still non-negligible, constituting up to 20% of the cross section [11].

The proper treatment of the collinear singularity considerably complicates the analytical computations both in the NNLO of CPM [12,47] and in the NLO of PRA, since in the PRA the part of transverse momentum is provided to the hard subprocess by the unPDFs. To avoid these difficulties, one can define the direct part of the cross section in the infrared-safe way, using the smooth-cone isolation condition [48]

$$r < R \Rightarrow E_T^{(\rm had)}(r) < E_T^{(\rm ISO)}\chi(r), \tag{10}$$

where $\chi(r) = (\frac{1-\cos(r)}{1-\cos(R)})^n$, $n \geq 1/2$. The isolation condition (10) is easy to implement into the process of Monte Carlo integration, and it makes the cross section of the subprocess (7) finite because the collinear singularities associated with the initial state are regularized by the unPDF. Applying the smooth-cone isolation to our calculation, we are completely eliminating the need in the fragmentation component [47,48], but of course this isolation does not match to the experimental one. However, as it was shown in Ref. [47], the cross section obtained with the isolation condition (10) is a lower estimate for the direct plus fragmentation cross section, obtained with the hard-cone isolation. Numerically, for $n = 1$, this estimate is very good, since it reproduces the NLO results with standard isolation with the accuracy of $O(1\%)$ [47]. Having in mind that we are going to discuss $O(50\% - 100\%)$ NLO effects, we will apply the isolation condition (10) to our present calculations.

The cross section of the subprocess (8) is also finite because the Sudakov form factor decreases in the region $q_T^2 \ll \mu^2$ faster than any positive power of q_T and therefore regularizes the collinear and soft singularities of the matrix element of the subprocess (8) in the limit of $q_{T5} \to 0$.

In the factorization formula (2), the part of the ISR, highly separated in rapidity from the particles produced in the hard subprocess, is included into unPDFs, and the effects of the additional radiations close in rapidity to the hard subprocess should be taken order by order in α_s in the hard-scattering coefficient. Therefore, the corresponding MRK asymptotics should be subtracted from the NLO QMRK contributions (7) and (8) to avoid the double counting, when the additional parton is highly separated in rapidity from the central region. The analogous procedure of the "localization in rapidity" of the QMRK contributions was proposed in Refs. [49,50]. To be compatible with our definition of the KMR unPDF (3), this subtraction term should interpolate smoothly between the strict MRK limit, when an additional parton goes deeply forward or backward in rapidity with fixed transverse momentum, and the collinear factorization limit, when the initial-state partons are nearly on shell and an additional parton has a small transverse momentum but its rapidity is arbitrary. Below, such a subtraction term is constructed in close analogy with the high-energy jets approach [51].

The Feynman diagrams for the subtraction terms, required for the squared amplitudes of the subprocesses (7) and (8) are shown in Fig. 5 and can be easily written according to the FRs of Fig. 1. To extend the applicability of the subtraction terms outside of the strict MRK limit, one has to implement the exact $2 \to 3$ kinematics for the subtraction terms, taking into account the exact $\hat{t}$-channel momentum in the propagator of the Reggeized quark. In what follows, we will refer to the amplitudes with the Reggeon propagators and vertices, but without kinematical approximations, characteristic for the MRK, as modified MRK (mMRK) amplitudes. As it was checked explicitly, the implementation of the exact kinematics does not destroy the gauge invariance of the subtraction terms with the Reggeized quarks in the $\hat{t}$ channels, presented in Fig. 5, as was the case for the mMRK amplitudes with the Reggeized gluons in the $\hat{t}$ channels in Ref. [51].

The last ambiguity, which we have to fix in the definition of our mMRK amplitudes, is the position of the $\hat{P}_\pm$-projector in the numerator of the propagator of the Reggeized quark. In the MRK limit, the small light-cone component of the Reggeon momentum can be neglected, and the projectors $\hat{P}_\pm$ commute with $\hat{q}_t$ under the sign of the trace, but outside of this limit, this is not true anymore. To fix this ambiguity, let us study the amplitudes of the

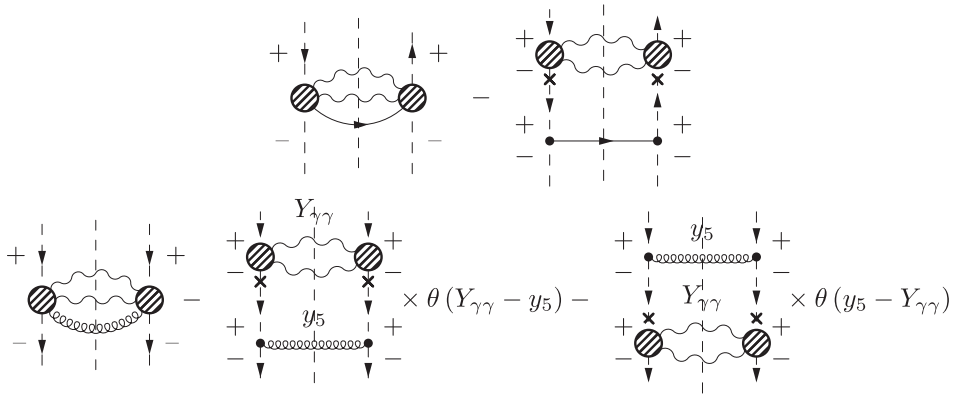

FIG. 5. Upper panel: the diagrammatic representation for the squared amplitude of the subprocess (7) and the corresponding mMRK subtraction term. Lower panel:- the same for the subprocess (8).

mMRK subprocesses in Fig. 6. Explicitly, they have the forms

$$\mathcal{A}^{ab}_{\mu\nu}(g\bar{Q}\to\bar{q}g) = g_s^2\bar{v}(q_2^{\parallel})\left(\gamma_\nu - \hat{q}_2\frac{n_\nu^+}{q_4^+} - \hat{q}_t\frac{n_\nu^-}{q_4^-}\right) \times T^b\hat{P}_+\frac{\hat{q}_t}{q_t^2}\left(\gamma_\mu - \hat{q}_t\frac{n_\mu^+}{q_1^+}\right)T^a v(q_3), \quad (11)$$

$$\mathcal{A}^{ab}_{\mu\nu}(q\bar{Q}\to gg) = g_s^2\bar{v}(q_2^{\parallel})\left(\gamma_\nu - \hat{q}_2\frac{n_\nu^+}{q_4^+} - \hat{q}_t\frac{n_\nu^-}{q_4^-}\right) \times T^b\hat{P}_+\frac{\hat{q}_t}{q_t^2}\left(\gamma_\mu + \hat{q}_t\frac{n_\mu^+}{q_3^+}\right)T^a u(q_1), \quad (12)$$

$$\mathcal{A}^{a}_{\mu}(Q\bar{Q}\to g) = g_s\bar{v}(q_2^{\parallel})\left(\gamma_\nu - \hat{q}_2\frac{n_\mu^+}{q_4^+} - \hat{q}_t\frac{n_\mu^-}{q_4^-}\right) \times T^a u(q_t^{\parallel}). \quad (13)$$

Taking the squared modulus of these amplitudes and averaging them over the initial-state spin and color quantum numbers, we get

$$\overline{|\mathcal{A}(g\bar{Q}\to\bar{q}g)|^2} = g_s^2\frac{\hat{s}+t_2}{\hat{s}+t_2+\hat{t}}\frac{2P_{qg}(z)}{z\hat{t}}\overline{|\mathcal{A}(Q\bar{Q}\to g)|^2}, \quad (14)$$

$$\overline{|\mathcal{A}(q\bar{Q}\to gg)|^2} = g_s^2\frac{\hat{s}+t_2}{\hat{s}+t_2+\hat{t}}\frac{2P_{qq}(z)}{z\hat{t}}\overline{|\mathcal{A}(Q\bar{Q}\to g)|^2}, \quad (15)$$

$$\overline{|\mathcal{A}(Q\bar{Q}\to g)|^2} = g_s^2\frac{C_A C_F}{N_c^2}(\mathbf{q}_{t\perp}^2 + t_2), \quad (16)$$

where $q_2^2 = -t_2$, the invariants $\hat{s}$, $\hat{t}$, $\hat{u}$ are defined after Eq. (6), $\mathbf{q}_{t\perp} = (\mathbf{q}_{T2} - \mathbf{q}_{T4})$, $z = 1 - q_3^+/q_1^+$, and $P_{qg}(z) = \frac{1}{2}(z^2 + (1-z)^2)$, $P_{qq}(z) = C_F\frac{1+z^2}{1-z}$ are the LO DGLAP splitting functions. Note that we have taken the limit $q_1^2 = 0$ to facilitate the study of the collinear singularity.

When $z \ll 1$ and $\hat{t}$ is fixed, the partons 3 and 4 are in the MRK. In the opposite (collinear) limit $\hat{t}\to 0$, the squared amplitudes (14), and (15) factorize into the collinear singularity with the corresponding DGLAP splitting function and the squared amplitude (16). From this example, one can conclude that the factor $\hat{q}_t$ should be taken together with the vertex of the MRK emission to correctly reproduce the collinear singularity of the amplitude. This prescription is denoted by the crosses on the quark propagators in Figs. 1, 5, and 6.

The squared amplitudes (14), (15) can also be used to explain the structure of the factorization formula (2) and the unPDF (3). The presence of the exact DGLAP splitting functions in (14) and (15) corresponds to the usage of the exact splitting functions in the unPDF (3). Factor z in the denominators of (14) and (15) is nothing but a flux factor of the $\hat{t}$-channel partons, which tells us that for the Reggeized partons one should use the same flux factor $I = 2Sx_1x_2$ as for the CPM partons. After the integration over the small light-cone component in the definition of the unPDF, the additional factor $1/(1-z)$ appears, which converts $\hat{t}$ into

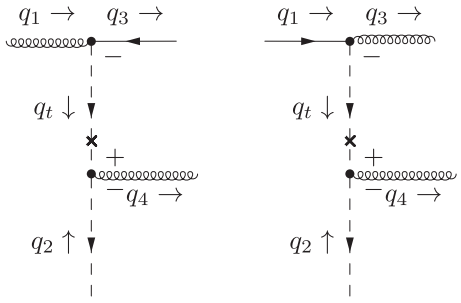

FIG. 6. The Feynman diagrams for the mMRK subprocesses $g(q_1) + \bar{Q}(q_2)\to\bar{q}(q_3) + g(q_4)$ (left panel) and $q(q_1) + \bar{Q}(q_2)\to g(q_3) + g(q_4)$ (right panel).

$\hat{t}(1-z) = \mathbf{q}_{t\perp}^2$, which is why the q_T^2 and not q^2 stands in the denominator of (3).

The rapidity ordering conditions are imposed in the subtraction terms for the subprocess (8) (see Fig. 5, lower panel), while for the case of the subprocess (7), the rapidity of the quark in the final state is unconstrained (Fig. 5, upper panel). This corresponds to the fact that in the KMR unPDF the radiation of the gluon is ordered in rapidity with the particles, produced in the hard subprocess, while for the quark, it is not the case. So, the mMRK terms constructed according to the Feynman diagrams in Fig. 5 are completely well defined and correspond to the definition of the unPDF (3).

IV. QUARK-BOX CONTRIBUTION

The subprocess

$$R(q_1) + R(q_2) \to \gamma(q_3) + \gamma(q_4) \tag{17}$$

is described by the quark-box amplitude and is formally NNLO $[O(\alpha^2\alpha_s^2)]$, but its contribution to the total cross section is expected to be comparable with NLO contributions, due to the enhancement by two gluon unPDFs. The $RR \to q\bar{q} + \gamma\gamma$ subprocess is also enhanced by two gluon PDFs. But it is reasonable to expect that its contribution will be negligible after the subtraction of double-counting contributions with LO and NLO because the leftover of such subtraction will be dominated by the $RR \to q(q \to \gamma) + \bar{q}(\bar{q} \to \gamma)$ double-fragmentation contribution. The latter is highly suppressed by the smallness of the double-fragmentation phase space and photon isolation conditions. In the present paper, we do not intend to do the complete NNLO computation in PRA, and in fact we include the box subprocess to our calculations, following the previous studies in k_T factorization [19,20] and the current experimental literature [3,4], where it is included together with the NLO contributions. It is of calculational and phenomenological interest to study the exact dependence of this contribution on the virtualities of initial-state partons.

The helicity amplitudes for the subprocess (17) could be written as

$$\mathcal{A}(RR, \lambda_3\lambda_4) = \frac{q_1^+ q_2^-}{4\sqrt{t_1 t_2}} n_{\mu_1}^- n_{\mu_2}^+ \varepsilon_{\mu_3}^\star(\lambda_3)\varepsilon_{\mu_4}^\star(-\lambda_4)\mathcal{M}^{\mu_1\mu_2\mu_3\mu_4}, \tag{18}$$

where λ_3, λ_4 are the helicities of the photons in the final state and the fourth-rank vacuum polarization tensor has the form

$$\mathcal{M}^{\mu_1\mu_2\mu_3\mu_4} = 2\int d^4q \left\{ \frac{\mathrm{tr}[(\hat{q}-\hat{q}_1)\gamma^{\mu_3}(\hat{q}+\hat{q}_2-\hat{q}_4)\gamma^{\mu_4}(\hat{q}+\hat{q}_2)\gamma^{\mu_2}\hat{q}\gamma^{\mu_1}]}{(q-q_1)^2(q+q_2-q_4)^2(q+q_2)^2q^2} + (q_3 \leftrightarrow q_4, \mu_3 \leftrightarrow \mu_4) + (q_2 \leftrightarrow -q_4, \mu_2 \leftrightarrow \mu_4) \right\}, \tag{19}$$

where the factor 2 takes into account the diagrams with the opposite direction of the fermion number flow. The following overall factor is taken out from the amplitude (18):

$$\frac{e^2 g_s^2}{(2\pi)^4}\frac{\delta_{ab}}{2}\left(\sum_q e_q^2\right).$$

We take the polarization vectors for the final-state photons in the form

$$\varepsilon^\mu(\lambda) = \frac{1}{\sqrt{2}}(n_x^\mu + i\lambda n_y^\mu),$$

where

$$n_x^\mu = \frac{1}{\Delta}((q_3q_4)q_2^\mu - (q_2q_4)q_3^\mu - (q_2q_3)q_4^\mu),$$
$$n_y^\mu = -\frac{1}{\Delta}\epsilon^{\mu q_2 q_3 q_4},$$

and $\Delta = \sqrt{\hat{s}\,\hat{t}\,\hat{u} - \hat{s}t_1t_2}/2$.

In Ref. [52], we managed to obtain the compact result for the helicity amplitudes of the process $\gamma R \to \gamma g$ and explicitly demonstrate the cancellation of the spurious collinear singularity $1/(t_1t_2)$ in the squared amplitude. For the process (17), it turns out to be impossible to obtain the reasonably compact results, and the actual task is to obtain the representation for the helicity amplitudes which will be useful for the numerical evaluation of the cross-section. To do this, we observe that, exploiting the Ward identity $q_{1,2}^{\mu_{1,2}}\mathcal{M}_{\mu_1\mu_2\mu_3\mu_4} = 0$ for the tensor (19), one can make the following substitutions in Eq. (17):

$$\frac{q_1^+ q_2^-}{4\sqrt{t_1t_2}}(n^-)^{\mu_1}(n^+)^{\mu_2} \to n_{T1}^{\mu_1} n_{T2}^{\mu_2},$$

where $n_{T1,2} = q_{T1,2}/\sqrt{t_{1,2}}$.

To get rid of the ϵ tensors and directly pass to the Passarino–Veltman reduction for the Feynman integrals with the scalar products in the numerator, we exploit the same trick as in Ref. [52]. We decompose the 4-vectors $n_{T1,2}$ as

$$n_{T1} = \beta_0^{(1)}q_1 + \beta_3^{(1)}q_3 + \beta_4^{(1)}q_4 + \gamma_1 n_y, \tag{20}$$

$$n_{T2} = \beta_0^{(2)}q_2 + \beta_3^{(2)}q_3 + \beta_4^{(2)}q_4 + \gamma_2 n_y, \tag{21}$$

and the vector n_y is introduced via its scalar products: $n_y^2 = -1$, $n_y q_2 = n_y q_3 = n_y q_4 = 0$. The coefficients of this decomposition can be straightforwardly expressed through the Mandelstam invariants, transverse momenta of particles, and azimuthal angles. After the Passarino–Veltman reduction, the helicity amplitudes were represented as linear combinations of two, three, and four-point scalar one-loop integrals, and the cancellation of the UV and IR divergences was checked both analytically and numerically. The coefficients of this decomposition depend on five invariants, $\hat{s}$, $\hat{t}$, $\hat{u}$, t_1, t_2, and eight coefficients, $\beta_i^{(j)}$, $\gamma_{1,2}$, i.e., 13 parameters in total. They can be represented as rational functions with tens of thousands of terms in the numerators. It turns out that just to reliably check the cancellation of the UV and IR divergences numerically one has to compute these coefficients with 30 digits of accuracy at least.

Also, it was checked, both analytically and numerically, that the collinear limit for the squared helicity amplitudes (18), defined as

$$\int_0^{2\pi} \frac{d\phi_1 d\phi_2}{(2\pi)^2} \lim_{t_{1,2}\to 0} |\mathcal{A}(RR, \lambda_3\lambda_4)|^2 = \frac{1}{4} \sum_{\lambda_{1,2}=\pm} |\mathcal{A}_{\mathrm{CPM}}(\lambda_1\lambda_2, \lambda_3\lambda_4)|^2,$$

holds, where the $|\mathcal{A}_{\mathrm{CPM}}(\lambda_1\lambda_2, \lambda_3\lambda_4)|^2$ is the squared helicity amplitude of the process $gg \to \gamma\gamma$ in the CPM. The numerical check of the collinear limit was performed by the technique described in Ref. [52]. The numerical results for the subprocess (17) will be presented in the next section, and the FORTRAN code for the calculation of the helicity amplitudes and differential cross sections of the process (17), as well as for the $2 \to 2$ subprocess (5) and $2 \to 3$ subprocesses (7) and (8), is available from the authors on request.

V. NUMERICAL RESULTS

The differential cross section of the $2 \to 2$ subprocesses (5), (17) can be represented as

$$\frac{d\sigma}{dq_{T3}dq_{T4}d\Delta\phi dy_3 dy_4} = \frac{1}{2!}\int dt_1 \int_0^{2\pi} d\phi_1 \sum_{ij} \Phi_i(x_1, t_1, \mu_F^2)\Phi_j(x_2, t_2, \mu_F^2) \frac{q_{T3}q_{T4}\overline{|\mathcal{A}_{ij}|^2}}{2(2\pi)^3 (Sx_1x_2)^2}, \tag{22}$$

where the factor $1/2!$ takes into account the identical nature of the photons, $q_{Ti} = |\mathbf{q}_{Ti}|$, y_i are the rapidities of the final-state particles, $\Delta\phi$ is the azimuthal angle between transverse momenta of the photons, ϕ_1 is the azimuthal angle between $\mathbf{q}_{T3}$ and $\mathbf{q}_{T1}$, $t_2 = (\mathbf{q}_{T3} + \mathbf{q}_{T4} - \mathbf{q}_{T1})^2$, and $x_{1,2} = (q_{T3}e^{\pm y_3} + q_{T4}e^{\pm y_4})/\sqrt{S}$. The spectra differential in the diphoton invariant mass (M) and diphoton transverse momentum $p_T = \sqrt{q_{T3}^2 + q_{T4}^2}$ could be obtained using the substitutions

$$dM = \frac{q_{T3}C}{M} dq_{T4}, \tag{23}$$

$$dp_T = \frac{D}{p_T} dq_{T4}, \tag{24}$$

where $C = \cosh(y_3 - y_4) - \cos(\Delta\phi)$, $D = \sqrt{p_T^2 - q_{T3}^2 \sin^2(\Delta\phi)}$, $q_{T4} = M^2/(2q_{T3}C)$ for the case of (23), and $q_{T4} = D - q_{T3}\cos(\Delta\phi)$ for the (24).

For the $2 \to 3$ subprocesses (7), (8), the formula for the differential cross section reads

$$\frac{d\sigma}{dq_{T3}dq_{T4}d\Delta\phi dy_3 dy_4 dy_5} = \frac{1}{2!}\int dt_1 \int_0^{2\pi} d\phi_1 \int dt_2 \int_0^{2\pi} d\phi_2 \times \sum_{ij} \Phi_i(x_1, t_1, \mu_F^2)\Phi_j(x_2, t_2, \mu_F^2) \frac{q_{T3}q_{T4}\overline{|\mathcal{A}_{ij}|^2}}{16(2\pi)^6 (Sx_1x_2)^2}, \tag{25}$$

and the differential cross sections over the p_T and M could be obtained using the substitutions (23) and (24) as in the $2 \to 2$ case.

For the numerical computations, we use the modified KMR unPDF (3) with the MSTW-2008 NLO PDFs [53] as the collinear input. Also, the value for the fine-structure constant $\alpha = 1/137.036$ was used in the calculations together with the NLO formula for the α_s with $\alpha_s(M_Z) = 0.12018$ and flavor thresholds at $m_c = 1.4$ GeV and $m_b = 4.75$ GeV. The choice of the factorization and renormalization scales $\mu_R = \mu_F = \xi M$ commonly used in the literature [3,4,11,12] was adopted, where the default value for $\xi = 1$ and the values $\xi = 2^{\pm 1}$ were used to estimate the scale uncertainty of the calculation, which

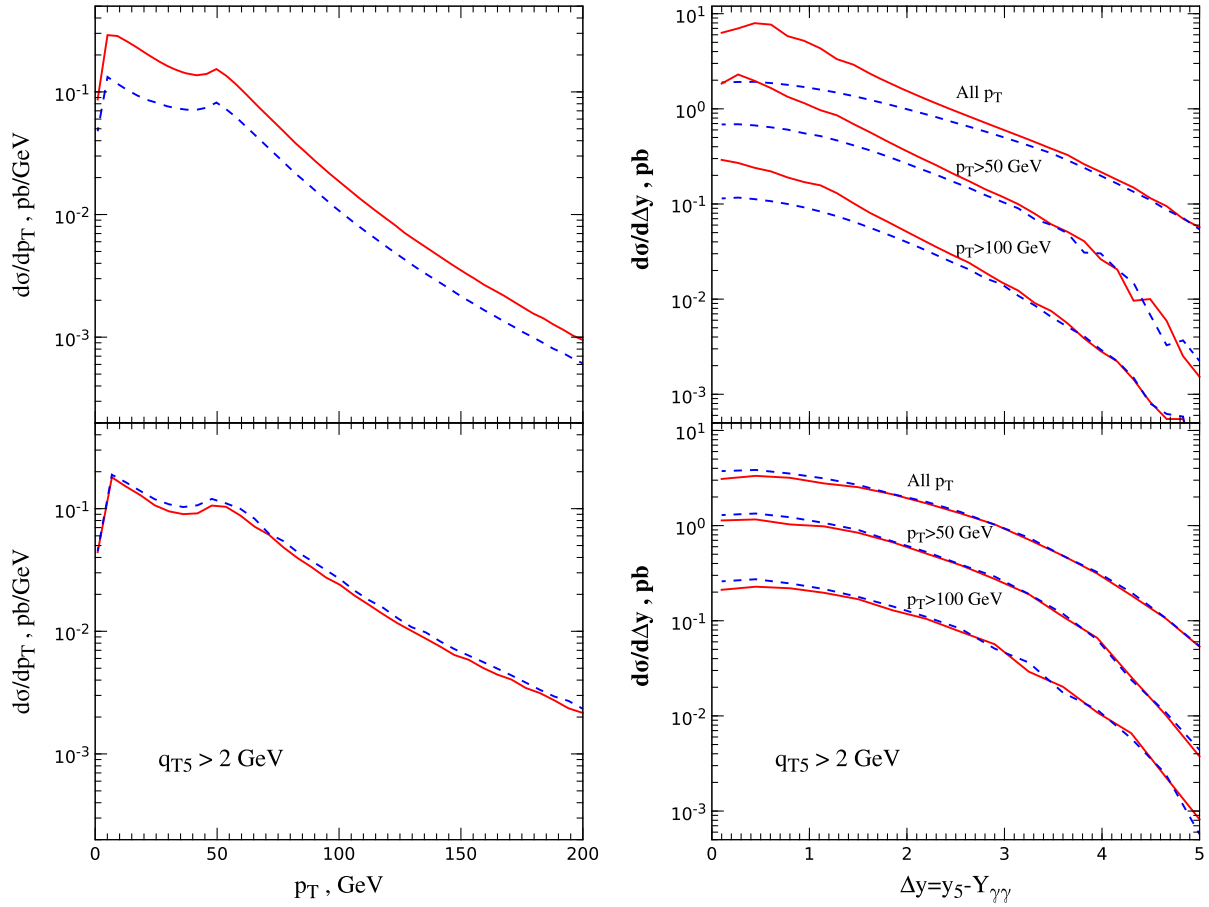

FIG. 7 (color online). The comparison of the p_T (left column) and Δy (right column) spectra for the NLO QMRK contributions (solid lines) with the corresponding mMRK subtraction terms (dashed lines). Upper panels: subprocess (7); lower panels: subprocess (8).

is indicated in Figs. 8–12 as the gray band. The numerical computations were performed mostly using the Suave adaptive Monte Carlo integration algorithm with the cross-checks against the results of Vegas and Divonne algorithms implemented in the CUBA library [54].

Before the presentation of the comparison of our calculations with experimental data, let us discuss the contribution of $2 \to 3$ subprocesses (7), (8) after the subtraction of double counting, discussed in Sec. III. In the left panel of Fig. 7, the p_T spectra for the NLO contributions (7), (8) in the ATLAS-2013 kinematical conditions (see the second column of Table I) is presented together with the corresponding mMRK subtraction contribution. For the CDF-2012 kinematics of Ref. [3] (first column of Table I), the qualitative picture is the same.

TABLE I. Kinematical conditions for the CDF and ATLAS data sets.

$p\bar{p}$, CDF-2012 [3]	pp, ATLAS-2013 [4]
$\sqrt{S} = 1960$ GeV	$\sqrt{S} = 7000$ GeV
$q_{T3,4} \geq 15,\ 17$ GeV	$q_{T3,4} \geq 22,\ 25$ GeV
$\lvert y_{3,4}\rvert \leq 1.0$	$\lvert y_{3,4}\rvert \leq 1.37,\ 1.52 \leq \lvert y_{3,4}\rvert \leq 2.37$
$R = 0.4,\ E_T^{(\mathrm{ISO})} = 2$ GeV	$R = 0.4,\ E_T^{(\mathrm{ISO})} = 4$ GeV

From Fig. 7, one can observe that the mMRK subtraction term reproduces the exact contribution of the NLO subprocess (8) with the 10% accuracy and constitutes more than 50% of the cross section of the subprocess (7) for the $p_T > 50$ GeV. As the right panel of Fig. 7 shows, for the subprocess (7), the significant deviation from the mMRK asymptotics starts only for $\Delta y = y_5 - Y_{\gamma\gamma} < 2.0$, while for the larger values of Δy, the QMRK $2 \to 3$ cross section is well described by the mMRK asymptotics. For the subprocess (8), the $2 \to 3$ cross section is reproduced by the mMRK approximation for all values of Δy. Consequently, more than 50% of the cross section of the subprocess (7) and almost all the contribution of the subprocess (8) will be canceled by the subtraction term. Having this in mind, we do not include the contribution of the subprocess (8) in the further calculations.

The squared amplitude for the subprocess (7) can be safely integrated from $q_{T5} = 0$ in (25). The cross section for the subprocess (8) is also finite, but for the small values of q_{T5}, most of the cross section is accumulated at $t_{1,2} \sim 1$ GeV^2, which is nothing other than the manifestation

of the usual infrared singularity for the radiation of the soft gluon. For this reason, the cutoff $q_{T5} > 2$ GeV was imposed to produce the lower panel of Fig. 7. The dependence of the cross section on the small-t behavior of the unPDF is unphysical and will be canceled away by the NLO real-virtual interference contribution.

Now, we are in a position to compare the predictions of our model with the experimental data of Refs. [3,4]. In the present study we concentrate on three main observables: $d\sigma/dp_T$, $d\sigma/d\Delta\phi$ and $d\sigma/dM$. The fixed-order calculations in the CPM are experiencing the greatest difficulties for $d\sigma/dp_T$ and $d\sigma/d\Delta\phi$, while $d\sigma/dM$ is the benchmark CPM observable, for which the multiscale nature of the process under consideration is less important. The comparison for the other observables will be discussed elsewhere.

In Fig. 8, the p_T spectra of the photon pair, measured by the CDF Collaboration, is presented. For this data set, three data samples are provided, the inclusive one and two data samples with the additional kinematical constraint $p_T < M$ or $p_T > M$ imposed. One can note that the inclusive data and data for the $p_T < M$ are well described for the $p_T > 25$ GeV by the sum of the LO contribution (5) and NLO contribution (7) after the mMRK subtraction. For the $p_T > M$, data are well described by our prediction for all values of p_T, and the NLO contribution is, in fact, negligible. The contribution of the box subprocess (17) is only about 15% of the cross section predicted at small p_T and decreases with p_T very quickly, contributing significantly only for the $p_T < 30$ GeV.

For $p_T < 25$ GeV, one can observe the deficit of the predicted cross section which reaches up to a factor of 5 at the $p_T = 7$ GeV. The region of small p_T corresponds to the kinematics of CPM, where the radiation of soft gluons and virtual corrections are dominating. We expect that the computation of the NLO real-virtual interference correction in the PRA will significantly reduce this gap. One of the advantages of PRA is that at NLO this correction is finite and can be considered separately from the real NLO corrections, which are the subject of the present study.

The good description of the data for the $p_T > M$ region supports the self-consistency of our approach, since the NLO correction in this region is almost canceled by the mMRK subtraction terms and the contribution of the real-virtual NLO correction is expected to be small here.

For the reader's convinience, in Figs. 8–12, we also have plotted the corresponding NLO CPM predictions. Data for these plots correspond to the `Diphox` predictions [11],

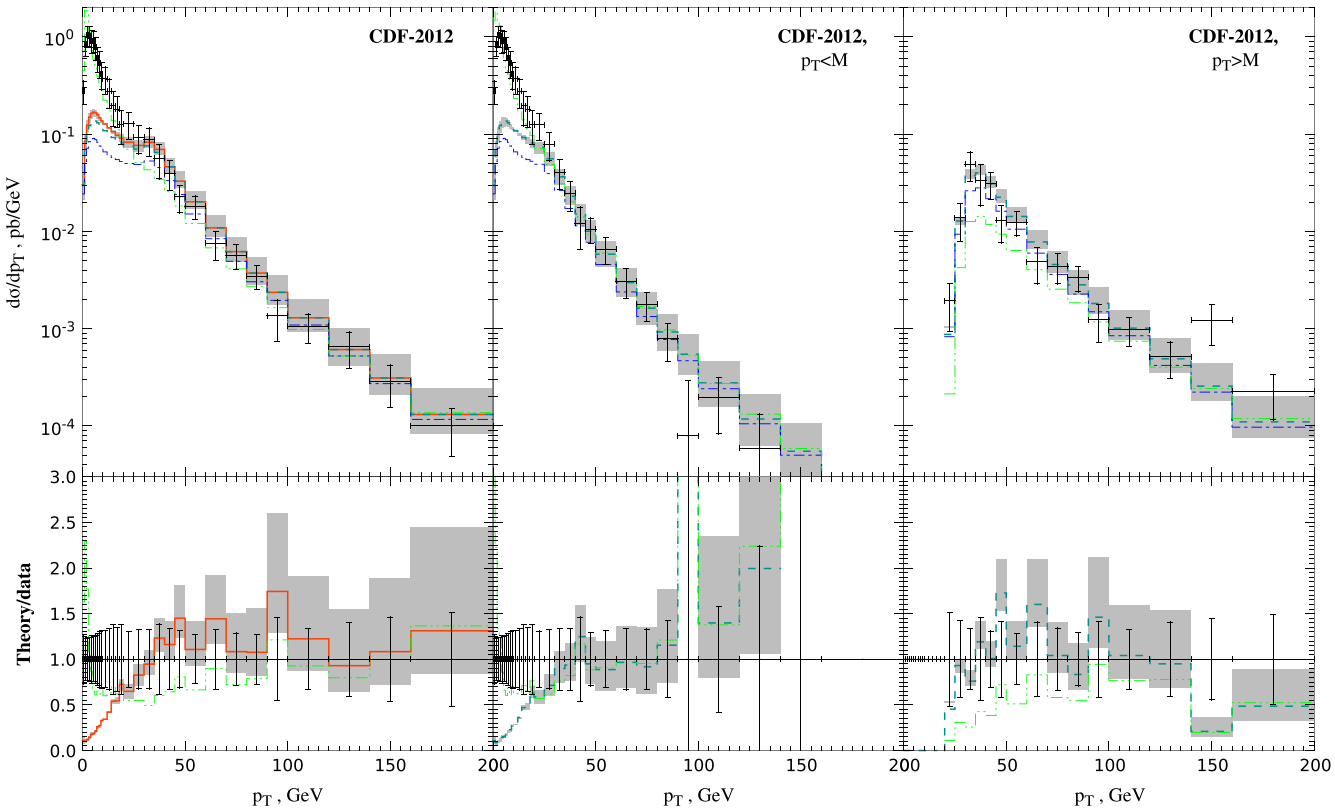

FIG. 8 (color online). The p_T spectra for the CDF-2012 data set. The thick solid curve is the sum of the contributions (5), (7) with mMRK subtraction and (17). The thick dashed curve is the sum of the first two. The thin dash-dotted curve is the contribution of the subprocess (5) only. The thin dash-double-dotted curve is the corresponding `Diphox` (NLO CPM) prediction, taken from Ref. [3]; see the text for details.

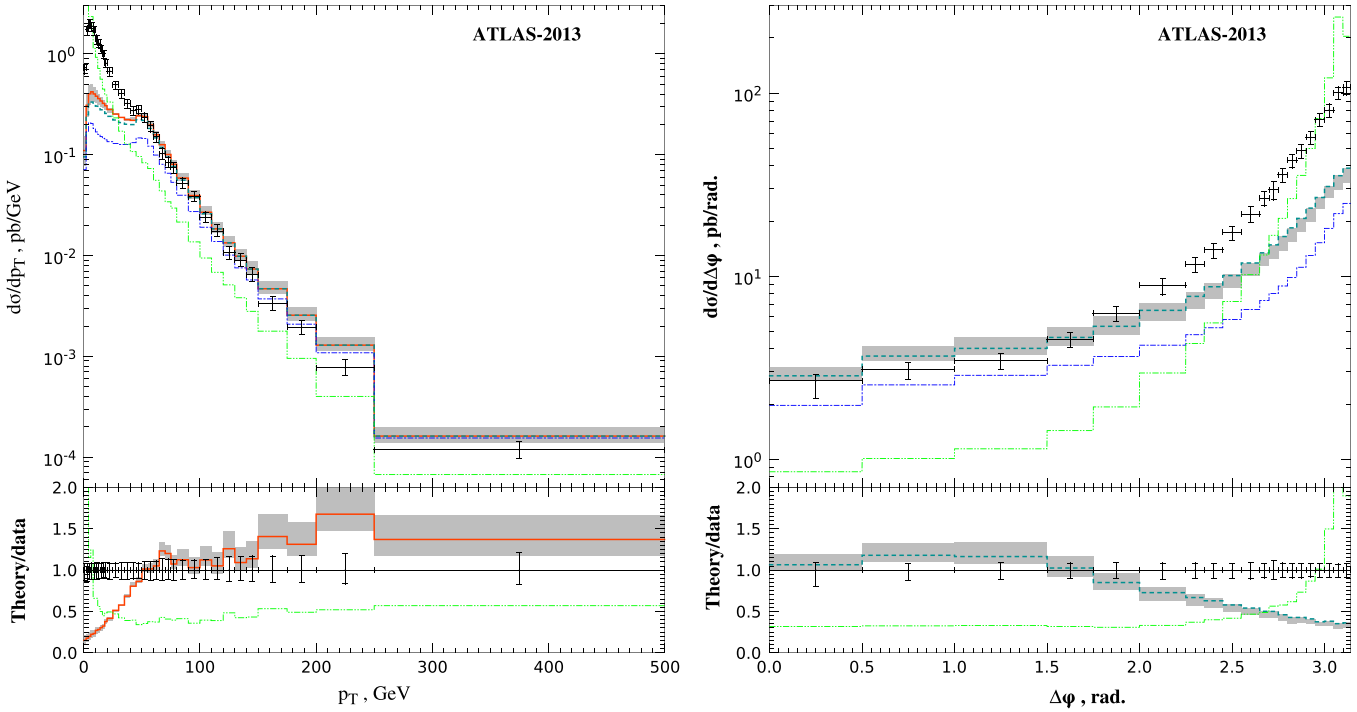

FIG. 9 (color online). The p_T spectra (left panel) and $\Delta\phi$ spectra (right panel) for the ATLAS-2013 data set. The notation for the curves is the same as in Fig. 8, except the thin dash-double-dotted curve, which is the `Diphox` (NLO CPM) prediction, taken from Ref. [4]; see the text for details.

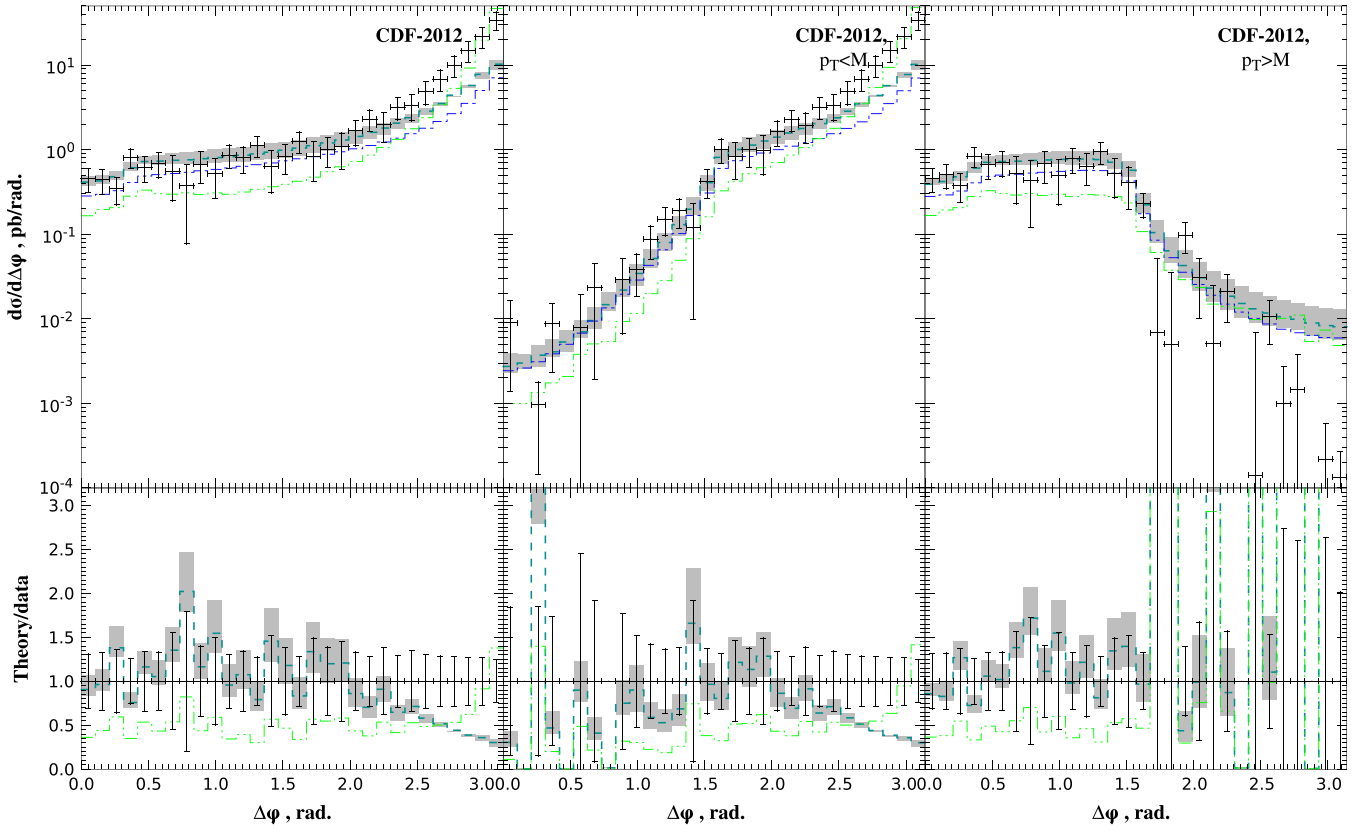

FIG. 10 (color online). The $\Delta\phi$ spectra for the CDF-2012 data set. The notation for the curves is the same as in Fig. 8.

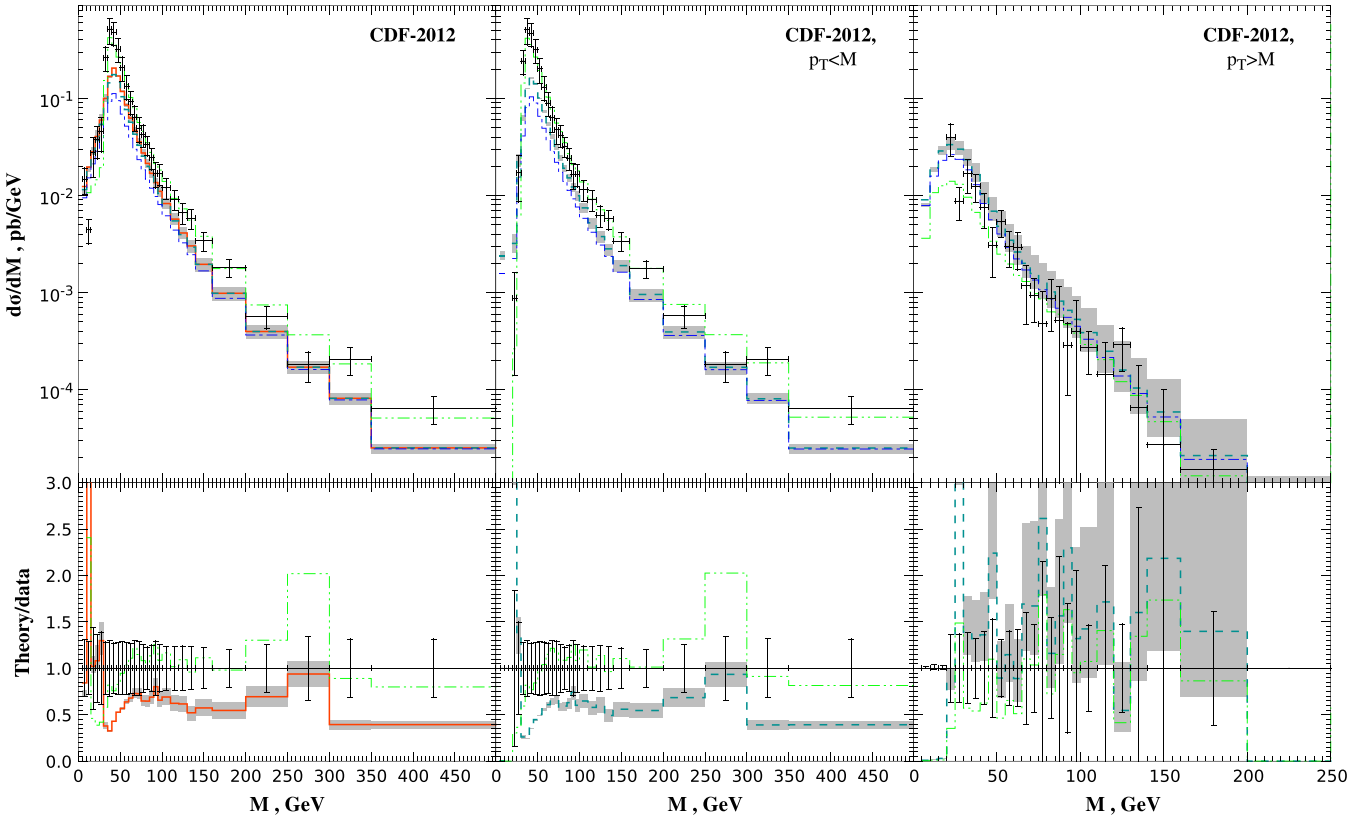

FIG. 11 (color online). Diphoton invariant mass spectra for the CDF-2012 data set. The notation for the curves is the same as in Fig. 8.

presented in the CDF [3] and ATLAS [4] experimental papers. The contribution of the $gg \to \gamma\gamma$ subprocess is also included into these predictions, via the GAMMA2MC program [24]. Comparing the NLO CPM and NLO* PRA predictions in Figs. 8–12, one can conclude that the NLO* approximation in PRA cannot describe the data on the $d\sigma/dM$ distribution due to the absence of the loop correction, which contributes mostly in the back-to-back CPM-like kinematics. But for the configurations far away from the CPM kinematics, the NLO* PRA describes the data substantially better than the NLO CPM, especially at the LHC. Moreover, in this region, the NLO* PRA prediction is dominated by the LO term, which demonstrates the better stability of PRA predictions for the kinematics far away from the CPM one. The inclusion of full NLO corrections should also improve the agreement in the CPM region.

In the left panel of Fig. 9, one can observe the same qualitative features as in the left panel of Fig. 8, despite the fact that we have moved from the Tevatron to the LHC with its 3.6 times larger energy and switched to pp collisions instead of $p\bar{p}$ ones. The NLO subprocess (7) is more important at the LHC than at the Tevatron, contributing significantly up to $p_T = 200$ GeV.

In Fig. 10 and right panel of Fig. 9, the $\Delta\phi$ spectra for the Tevatron and LHC are presented. In both figures, one can observe a good agreement of our predictions with data for

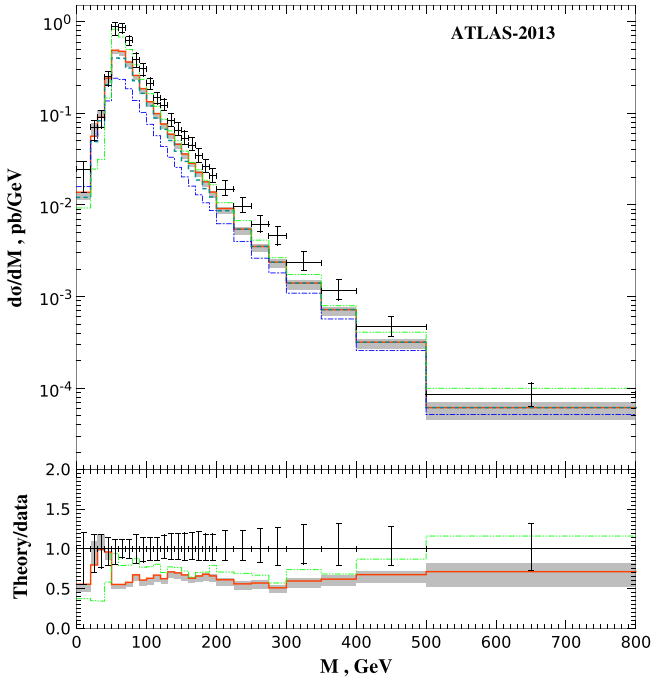

FIG. 12 (color online). Diphoton invariant mass spectrum for the ATLAS-2013 data set. The notation for the curves is the same as in Fig. 8.

$\Delta\phi < 1.5$ which corresponds to the high deviation from the back-to-back kinematics for the photons. In this region, the NLO correction is manifestly subleading, as it was for the p_T spectrum. The good description of the Tevatron data for the $p_T > M$ case is also there, as well, as the deficit of the predicted cross section for the back-to-back kinematics.

As for the M spectra of Figs. 11 and 12, one certainly expects the deficit of the calculated cross section for the most values of M due to the deficit of the cross section for the CPM kinematics, observed earlier, since most of the total cross section is accumulated near the CPM configurations. However, in the region of M below the peak, the data are well described, demonstrating that the PRA is suitable for the description of the effects of kinematical cuts. Once again, we observe the good description of the M spectrum for the $p_T > M$ subset of the Tevatron data.

The contribution of the quark-box subprocess (17) to the M spectra is found to be only about 8% of the observed cross section in the peak and 18% of the predicted cross section, both for the CDF-2012 and ATLAS-2013 kinematics. This result is 20%–30% smaller than the usual CPM estimate [12], which is in accordance with the findings of Ref. [52], where it was shown that the spacelike virtuality of the initial-state partons suppresses the $\gamma R \to \gamma g$ contribution with respect to the CPM expectation.

VI. CONCLUSIONS

In the present study, the pair hadroproduction of prompt photons is considered in the framework of the PRA with tree-level NLO corrections (7), (8) and the NNLO quark-box subprocess (17) taken into account. The procedure of localization in the rapidity of the tree-level NLO corrections to avoid double counting the real emissions between the hard-scattering part of the cross section and unPDF is proposed in Sec. III. As a consequence of this procedure, the real NLO corrections were put under quantitative control, and their contribution was found to be numerically small at high p_T or in the kinematical region $p_T > M$. The kinematical region $p_T > M$ is interesting for the further theoretical and experimental study, as an ideal testing site for the PRA, where the MRK between the ISR and the hard subprocess is dominating. The contribution of the quark-box subprocess (17) was found to be about 8% of the observed cross section in the peak of the $d\sigma/dM$ distribution, which is a bit smaller than the CPM estimate [12] due to the spacelike virtuality of the initial-state partons, similarly to the results of Ref. [52].

ACKNOWLEDGMENTS

This work was supported by Russian Foundation for Basic Research through the Grant No. 14-02-00021 and by the Ministry of Education and Science of Russia under Competitiveness Enhancement Program of SSAU for 2013-2020. The work of M. A. N. was also supported by the Graduate Students Scholarship Program of the Dynasty Foundation. The authors would like to thank M. G. Ryskin, G. Watt, and E. de Oliveira for providing to us their numerical codes for the calculation of the KMR unPDF of Ref. [42]. M. A. N. would like to thank the Department of the Phenomenology of the Elementary Particles of the II Institute for Theoretical Physics of Hamburg University and personally B. A. Kniehl for their kind hospitality during the initial stage of this work and the computational resources provided.

[1] G. Aad *et al.* (ATLAS Collaboration), Phys. Lett. B **716**, 1 (2012); S. Chatrchyan *et al.* (CMS Collaboration), Phys. Lett. B **716**, 30 (2012).
[2] G. Aad *et al.* (ATLAS Collaboration), Phys. Rev. Lett. **113**, 171801 (2014).
[3] T. Aaltonen *et al.* (CDF Collaboration), Phys. Rev. D **84**, 052006 (2011); Phys. Rev. Lett. **110**, 101801 (2013).
[4] G. Aad *et al.* (ATLAS Collaboration), J. High Energy Phys. 01 (2013) 086.
[5] T. Aaltonen *et al.* (CDF Collaboration), Phys. Rev. D **80**, 111106 (2009).
[6] G. Aad *et al.* (ATLAS Collaboration), Phys. Rev. D **89**, 052004 (2014).
[7] S. Chatrchyan *et al.* (CMS Collaboration), Phys. Rev. D **84**, 052011 (2011).
[8] S. Catani, M. Fontannaz, J. P. Guillet, and E. Pilon, J. High Energy Phys. 05 (2002) 028; P. Aurenche, M. Fontannaz, J. P. Guillet, E. Pilon, and M. Werlen, Phys. Rev. D **73**, 094007 (2006).
[9] V. A. Saleev, Phys. Rev. D **78**, 034033 (2008).
[10] B. A. Kniehl, V. A. Saleev, A. V. Shipilova, and E. V. Yatsenko, Phys. Rev. D **84**, 074017 (2011).
[11] T. Binoth, J. P. Guillet, E. Pilon, and M. Werlen, Eur. Phys. J. C **16**, 311 (2000).
[12] S. Catani, L. Cieri, D. de Florian, G. Ferrera, and M. Grazzini, Phys. Rev. Lett. **108**, 072001 (2012).
[13] J. C. Collins, *Foundations of Perturbative QCD* (Cambridge University Press, Cambridge, England, 2011).
[14] T. Becher, M. Neubert, and D. Wilhelm, J. High Energy Phys. 02 (2012) 124.
[15] M. Anselmino, M. Boglione, J. O. Gonzalez Hernandez, S. Melis, and A. Pokudin, J. High Energy Phys. 04 (2014) 005.
[16] F. Landry, R. Brock, P. M. Nadolsky, and C. P. Yuan, Phys. Rev. D **67**, 073016 (2003).

[17] L. V. Gribov, E. M. Levin, and M. G. Ryskin, Phys. Rep. **100**, 1 (1983); J. C. Collins and R. K. Ellis, Nucl. Phys. **B360**, 3 (1991); S. Catani, M. Ciafaloni, and F. Hautmann, Nucl. Phys. **B366**, 135 (1991).
[18] M. Ciafaloni, Nucl. Phys. **B296**, 49 (1988); S. Catani, F. Fiorani, and G. Marchesini, Nucl. Phys. **B336**, 18 (1990); Phys. Lett. B **234**, 339 (1990); G. Marchesini, Nucl. Phys. **B445**, 49 (1995).
[19] V. A. Saleev, Phys. Rev. D **80**, 114016 (2009).
[20] A. V. Lipatov, J. High Energy Phys. 02 (2013) 009; 02 (2013) 009.
[21] E. L. Berger, E. Braaten, and R. D. Field, Nucl. Phys. **B239**, 52 (1984).
[22] D. Acosta *et al.* (CDF Collaboration), Phys. Rev. Lett. **95**, 022003 (2005).
[23] V. Costantini, B. De Tollis, and G. Pistoni, Nuovo Cimento A **2**, 733 (1971); V. N. Baier, V. S. Fadin, V. M. Katkov, and E. A. Kuraev, Phys. Lett. B **49**, 385 (1974).
[24] Z. Bern, L. J. Dixon, and C. Schmidt, Phys. Rev. D **66**, 074018 (2002).
[25] J. C. Collins, D. E. Soper, and G. F. Sterman, Nucl. Phys. **B261**, 104 (1985); G. T. Bodwin, Phys. Rev. D **31**, 2616 (1985); **34**, 3932 (1986); **34**, 3932(E) (1986).
[26] L. N. Lipatov, Yad. Fiz. **23**, 642 (1976) [Sov. J. Nucl. Phys. **23**, 338 (1976)]; E. A. Kuraev, L. N. Lipatov, and V. S. Fadin, Zh. Eksp. Teor. Fiz. **71**, 840 (1976) [Sov. Phys. JETP **44**, 443 (1976)]; Zh. Eksp. Teor. Fiz. **72**, 377 (1977) [Sov. Phys. JETP **45**, 199 (1977)]; I. I. Balitsky and L. N. Lipatov, Yad. Fiz. **28**, 1597 (1978) [Sov. J. Nucl. Phys. **28**, 822 (1978)]; Zh. Eksp. Teor. Fiz. **90**, 1536 (1986) [Sov. Phys. JETP **63**, 904 (1986)].
[27] L. N. Lipatov, Phys. Rep. **286**, 131 (1997).
[28] B. L. Ioffe, V. S. Fadin, and L. N. Lipatov, *Quantum Chromodynamics: Perturbative and Nonperturbative Aspects* (Cambridge University Press, Cambridge, England, 2010).
[29] V. S. Fadin and V. E. Sherman, JETP Lett. **23**, 599 (1976); JETP Lett. **45**, 861 (1977).
[30] A. V. Bogdan and V. S. Fadin, Nucl. Phys. **B740**, 36 (2006).
[31] L. N. Lipatov, Nucl. Phys. **B452**, 369 (1995).
[32] L. N. Lipatov and M. I. Vyazovsky, Nucl. Phys. **B597**, 399 (2001).
[33] E. N. Antonov, L. N. Lipatov, E. A. Kuraev, and I. O. Cherednikov, Nucl. Phys. **B721**, 111 (2005).
[34] A. van Hameren, K. Kutak, and T. Salwa, Phys. Lett. B **727**, 226 (2013).
[35] A. van Hameren, J. High Energy Phys. 07 (2014) 138.
[36] V. N. Gribov and L. N. Lipatov, Yad. Fiz. **15**, 781 (1972) [Sov. J. Nucl. Phys. **15**, 438 (1972)]; Yu. L. Dokshitzer, Zh. Eksp. Teor. Fiz. **73**, 1216 (1977) [Sov. Phys. JETP **46**, 641 (1977)]; G. Altarelli and G. Parisi, Nucl. Phys. **126**, 298 (1977).
[37] J. Blümlein, DESY Report No. 95-121 (1995).
[38] M. A. Kimber, A. D. Martin, and M. G. Ryskin, Eur. Phys. J. C **12**, 655 (2000); Phys. Rev. D **63**, 114027 (2001); G. Watt, A. D. Martin, and M. G. Ryskin, Eur. Phys. J. C **31**, 73 (2003); Phys. Rev. D **70**, 014012 (2004); **70**, 079902(E) (2004).
[39] A. V. Karpishkov, M. A. Nefedov, V. A. Saleev, and A. V. Shipilova, Phys. Rev. D **91**, 054009 (2015).
[40] A. V. Karpishkov, M. A. Nefedov, V. A. Saleev, and A. V. Shipilova, Int. J. Mod. Phys. A **30**, 1550023 (2015).
[41] F. Hautmann, H. Jung, M. Krämer, P. J. Mulders, E. R. Nocera, T. C. Rogers, and A. Signori, Eur. Phys. J. C **74**, 3220 (2014).
[42] A. D. Martin, M. G. Ryskin, and G. Watt, Eur. Phys. J. C **66**, 163 (2010).
[43] The singularity of the $P_{gg}(z)$ splitting function at $z \to 0$ is also regularized by the cutoff $\theta(z - 1 + \Delta_{gg})$ in (3) and (4), which is not shown there for brevity. See Ref. [42] for the details.
[44] See Supplemental Material at http://link.aps.org/supplemental/10.1103/PhysRevD.92.094033 to obtain the `ReggeQuarks` model file, its usage instructions, and examples, including the $2 \to 2$ and $2 \to 3$ tree-level amplitudes used in this paper.
[45] T. Hahn, Comput. Phys. Commun. **140**, 418 (2001).
[46] R. Mertig, M. Bohm, and A. Denner, Comput. Phys. Commun. **64**, 345 (1991).
[47] L. Cieri and D. de Florian, arXiv:1405.1067.
[48] S. Frixione, Phys. Lett. B **429**, 369 (1998).
[49] J. Bartels, A. Sabio Vera, and F. Schwennsen, J. High Energy Phys. 11 (2006) 051.
[50] M. Hentschinski and A. S. Vera, Phys. Rev. D **85**, 056006 (2012).
[51] J. R. Andersen, V. Del Duca, and C. D. White, J. High Energy Phys. 02 (2009) 015; J. R. Andersen and J. M. Smillie, J. High Energy Phys. 01 (2010) 039.
[52] B. A. Kniehl, M. A. Nefedov, and V. A. Saleev, Phys. Rev. D **89**, 114016 (2014).
[53] A. D. Martin, W. J. Stirling, R. S. Thorne, and G. Watt, Eur. Phys. J. C **63**, 189 (2009).
[54] T. Hahn, Comput. Phys. Commun. **168**, 78 (2005).